Experiments on Magnetic-Field-Line Reconnection

R. L. Stenzel and W. Gekelman
Department of Physics, University of California, Los Angeles, California 90024
(Received 12 February 1979)

In a very large laboratory plasma the process of magnetic-field-line reconnection has been diagnosed carefully. The temporal evolution of a narrow ($\sim 3c/\omega_{pe}$) neutral layer with Petschek slow shocks is observed. Electrostatic fields are found to be as important as induced electric fields.

The reconnection of magnetic field lines near a neutral point is a problem of fundamental importance in space plasmas[1] (e.g., solar flares, substorms) as well as in some fusion plasmas (e.g., tearing modes in tokamaks). However, in neither of these cases are detailed *in situ* measurements possible. We have therefore built a large, weakly collisional, high-beta research laboratory plasma to explore the physics of the reconnection process. Such experiments have been pursued earlier in pinches[2-4] but, unfortunately, the effects were collision dominated and/or difficult to diagnose. In the present Letter we show the first detailed pictures of slow shocks near a neutral sheet predicted by Petschek.[5]

The experiment is performed in a linear device (Fig. 1) in which a large (~1-m-diam, 2-m-length), uniform, low-pressure (~10^{-4}-Torr) discharge plasma is produced with an oxide-coated cathode and adjacent mesh anode. The pulsed argon plasma ($n_e \simeq 10^{12}$ cm^{-3}, $T_e \simeq 10 T_i \simeq 4$ eV, 0.8-sec repetition rate, 1% duty cycle) is immersed in a constant, uniform, axial bias magnetic field ($B_0 \simeq 20$ G, plasma $\beta = 0.4$). A time-dependent transverse magnetic field [Fig. 1(b)] is established by pulsing an axial current ($\lesssim$ 20-kA peak, ~100-μsec rise time) through two parallel copper electrodes (60 cm wide, 150 cm long, 30-cm spacing). The current returns via the metallic chamber walls. The vacuum field geometry contains an X-type neutral point on the axis of the device, closed (private) flux inside the separatrix encircling each conductor, and, dominantly, common flux outside the separatrix. The peak common magnetic field exceeds the bias magnetic field by a factor 2 to 10. Associated with the time-varying transverse magnetic field is an axial electric field $E_y = -\dot{A}_y \equiv -\partial A_y/\partial t$ ($\vec{A}$ is the vector potential, $\vec{B} = \nabla \times \vec{A}$). In the presence of plasma the electric field gives rise to axial currents carried dominantly by electrons drifting from the cathode end to the opposing grounded chamber wall. The current closes via the walls to the cathode which emits as many electrons as are collected at the end plate. The plasma currents modify the magnetic field topology and the electric fields which, in turn, determine the current, and hence the system evolves self-consistently.

The net electric field in the plasma consists of the sum of induced and space-charge electric fields, $\vec{E} = -\dot{\vec{A}} - \nabla\varphi$. All three terms have been measured directly. The induced field is obtained with a loop probe consisting of two parallel wires in the radial x direction connected by a short ($\Delta y = 3.8$ cm) axial wire along the neutral line. Thus, the loop links over a distance Δy the total common flux ψ. The open-loop voltage V outside the diameter is given by

$$V = -\dot{\psi} = -\int \dot{B}_z \, dx \, \Delta y = -\oint \dot{\vec{A}} \cdot d\vec{l} = -\dot{A}\Delta y,$$

and hence $\dot{A} = -V/\Delta y$. Figure 2(a) shows the induced fields in vacuum and with plasma. The applied wave form in vacuum is governed by circuit parameters (R, L, C). Typical peak values are

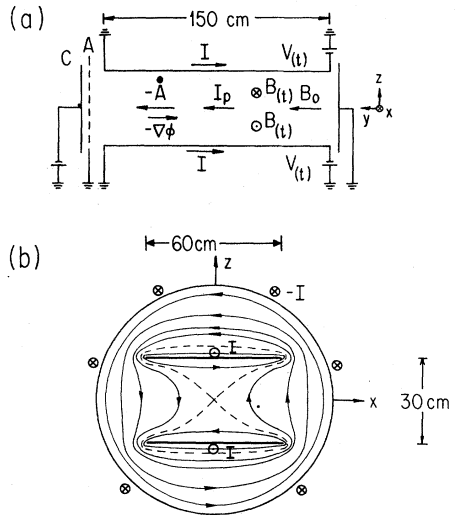

FIG. 1. (a) Schematic side view and (b) axial view of the experimental setup.

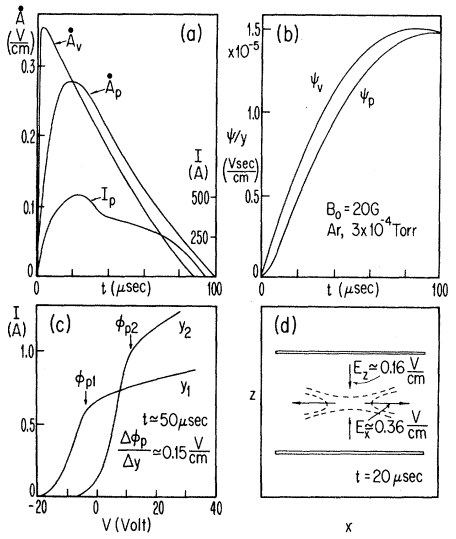

FIG. 2. (a) Induced electric fields and plasma current I_p. (b) Common flux in vacuum and plasma. (c) Langmuir-probe traces at different axial positions. (d) Transverse electrostatic fields.

$0 < \dot{A}_v < 1$ V/cm. In the space between the copper electrodes $\dot{A}_v$ is nearly uniform. In the presence of plasma the magnetic field of the plasma current I_p is superimposed on the vacuum field. Flux changes due to the time-varying current $I_p(t)$ cause the difference in observed fields, $\dot{A}_v - \dot{A}_p = \dot{\psi}_p/\Delta y \simeq L_p \dot{I}_p/\Delta y$ (L_p is the plasma inductance). The total common flux per length Δy is readily found by time integration, $\psi/\Delta y = \int \dot{A}\, dt = A$. Figure 2(b) shows the reduced flux buildup in the presence of plasma. From the difference $\Delta\psi = \psi_v - \psi_p$ and the plasma current, one obtains the magnetic energy stored in the plasma, $W = \frac{1}{2}\Delta\psi I_p \simeq 7\times10^{-2}$ J ($t \simeq 60$ μsec).

The electrostatic field is obtained from gradients in the plasma potential. Floating-potential measurements are found unreliable because of the presence of energetic electrons. Using two radially inserted Langmuir probes, we observe [Fig. 2(c)] axial electrostatic fields in opposite direction to the induced field and of comparable magnitude, $|\nabla\varphi| \lesssim \dot{A}$. Thus, the total axial electric field is much smaller than the applied field. The latter can be raised well above the Dreicer field, and yet the observed electron drift velocity determined with differential one-sided Langmuir probes remains $v_d/v_e \lesssim 0.2$. In order to perform a careful difference measurement, an L-shaped probe has been constructed which is inserted radially along x and has a $\Delta y = 10$ cm long axial extension parallel to $\dot{A}$ so that a voltage $\dot{A}\Delta y$ is induced on it. By rotation of the radial shaft through 180° the plasma potential φ_p is measured at two axial points along the neutral line and the local induced electric field is automatically subtracted, $E_y = |\Delta\varphi_p/2\Delta y| - |\dot{A}_y|$. These measurements yield typically $E_y \simeq 70$ mV/cm when $\dot{A} \simeq 300$ mV/cm with E_y in the direction of $-\dot{A}$. With the measured current density ($j_y \lesssim 3$ A/cm^2), the resistivity $\eta = E_y/j_y \simeq 23$ mΩ cm is only moderately enhanced over the classical Spitzer value ($\eta \simeq 13$ mΩ cm at 5 eV, 10^{12} cm^{-3}). Sampled Langmuir-probe traces indicate only minor electron heating ($\Delta kT_e \simeq 1$ eV) as expected in the absence of significant anomalous resistivity.

Space-charge electric fields also arise in the transverse x-z plane as a result of electron $\vec{E}_y \times \vec{B}$ motion and the fact that ions are unmagnetized. Figure 2(d) summarizes the results of $\nabla_\perp\varphi_p$ measurements. The electric fields point vertically into the neutral region and horizontally outward. These fields accelerate the ions and can be taken as a measure for the fluid drifts. Since $E_\perp \gg E_\parallel$, fluid motions are dominantly transverse. Direct measurements of the mass motion have been performed with orthogonal double-sided ion energy analyzers. These results will be published later.

In the problem of field reconnection, the magnetic field topology is of prime interest. Using two orthogonal magnetic loops we measure, at a fixed position (x, z), the temporal development of the transverse magnetic field. Because of the high repetition rate (1 Hz) and good reproducibility ($\simeq 10\%$) we perform such measurements at several hundred points in the transverse plane. The data acquired by a transient recorder are fed on line into a computer which subsequently plots vector maps, contour maps, and topological views of magnetic fields or currents at any desired instant of time. Figure 3 shows two examples of direction and magnitude of $\vec{B}_{(t)}$, one at an early time [Figs. 3(a) and 3(b), $t = 20$ μsec $\gtrsim$ Alfvén transit time from copper conductors to neutral line], and a second one at $t = 60$ μsec [Figs. 3(c) and 3(d)] which is the stationary result as long as the external current rises ($t_{\text{rise}} \simeq 100$ μsec; magnetic field diffusion time $t_{\text{dif}} \simeq 300$ μsec). At early times an X-point field geometry is clearly visible although the field lines are much straighter in the x direction than in the case of the vacuum field where the separatrix intersects at right angles. This flattening process continues and a broad neutral sheet

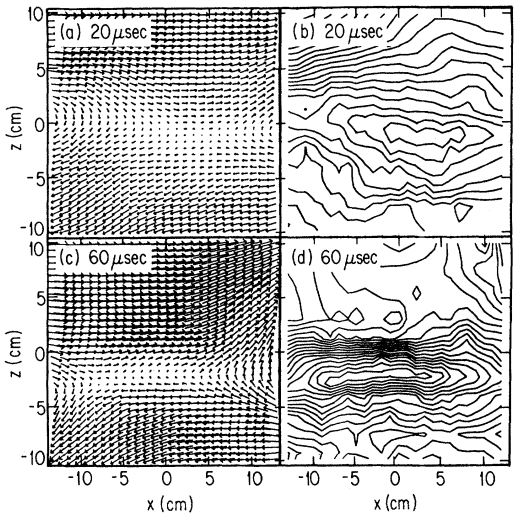

FIG. 3. (a), (c) Vector maps of measured magnetic fields and (b), (d) contours of constant $|\vec{B}|$ at different times during the current rise.

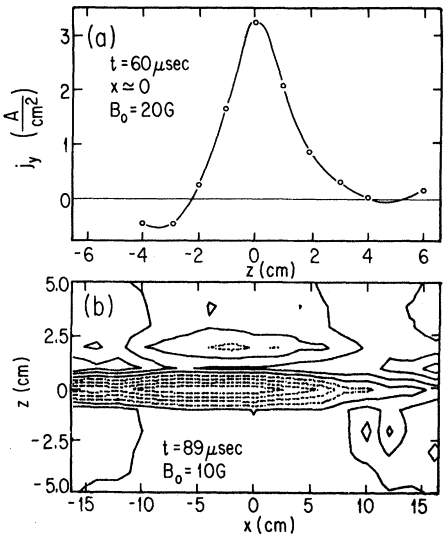

FIG. 4. (a) Measured current density across neutral sheet. (b) Contours of constant j_y calculated from the measured transverse fields, $j_y = (\nabla \times \vec{B})_y/\mu_0$.

evolves (Fig. 3; note different scales for x and z). Furthermore, from the contours of constant magnitude of B [Figs. 3(b) and 3(d)] one can see the evolution of slow shocks, i.e., steep gradients in B on either side ($\pm z$) of the neutral sheet. The full width of the neutral sheet ($\Delta z \simeq 2$ cm, after taking the spatial probe response into account) corresponds to approximately three collisionless skin depths ($c/\omega_{pe} \simeq 6$ mm) which is comparable to the distance at which the magnetic Reynolds number equals unity. In a second experiment at a reduced bias field ($B_0 = 10$ G), the neutral sheet was even thinner (1.5 cm) and longer (20 cm).

Finally, we have investigated the current distribution both by *in situ* measurements and by derivation from the magnetic field measurements ($\vec{j} = \nabla \times \vec{B}/\mu_0$). The first technique involves a differential Langmuir probe consisting of two equal one-sided plane collectors (3 mm × 4 mm) drawing electron saturation current in the $\pm y$ direction. The difference current yields directly the local current density j_y in magnitude and direction. Figure 4(a) shows the observed current profile across the neutral sheet at one instant of time. These direct measurements are consistent with calculations from $\nabla \times \vec{B}$ shown in Fig. 4(b). Both data confirm the sheetlike current structure. During the evolution of the neutral sheet the current distribution is rather complicated, exhibiting propagation of current channels, return currents, and significant fluctuations.

The authors gratefully acknowledge helpful discussions with F. Coroniti, the generously given computational assistance from J. Leboeuf and M. Thaker, and expert technical support from M. Plummer. This work was supported by National Science Foundation Grants No. ATM-77-18736 and No. ATM 77-23139.

[1]V. M. Vasyliunas, Rev. Geophys. Space Phys. 13, 303 (1975).

[2]A. Bratenahl and C. M. Yeates, Phys. Fluids 13, 2696 (1970); P. J. Baum, A. Bratenahl, M. Kao, and R. S. White, Phys. Fluids 16, 1051 (1973).

[3]S. I. Syrovatskii, A. G. Frank, and A. Z. Khodzhaev, Zh. Tekh. Fiz. 43, 912 (1973) [Sov. Phys. Tech. Phys. 18, 580 (1973)].

[4]J. Ohyabu, S. Okamura, and N. Kawashima, J. Geophys. Res. 79, 1977 (1974).

[5]H. E. Petschek, in *Proceedings of the AAS-NASA Symposium on the Physics of Solar Flares, Goddard Space Flight Center, Greenbelt, Maryland, 1963*, edited by W. N. Hess, U. S. National Bureau of Standards Special Publication No. SP50 (U. S. GPO, Washington, D. C., 1964), p. 425; see also Ref. 1, p. 310.